

Transfer excitation reactions in fast proton-helium collisions

M. S. Schöffler^{1,*}, H.-K. Kim¹, O. Chuluunbaatar^{2,3}, S. Houamer⁴,

A.G. Galstyan⁵, J. N. Titze¹, T. Jahnke¹, L. Ph. H. Schmidt¹,

H. Schmidt-Böcking¹, R. Dörner¹, Yu. V. Popov⁶, and A. A. Bulychev²

¹ *Institut für Kernphysik, Universität Frankfurt,*

Max-von-Laue-Str. 1, 60438 Frankfurt, Germany

² *Joint Institute for Nuclear Research,*

Dubna, Moscow region 141980, Russia

³ *School of Mathematics and Computer Science,*

National University of Mongolia, Ulaanaatar, Mongolia

⁴ *Département de physique, Faculté des Sciences,*

Université Ferhat Abbas, Sétif, 19000, Algeria

⁵ *Faculty of Physics, Lomonosov Moscow State University, Moscow 119991, Russia and*

⁶ *Skobeltsyn Institute of Nuclear Physics,*

Lomonosov Moscow State University, Moscow 119991, Russia

(Dated: May 29, 2022)

Abstract

Continuing previous work, we have measured the projectile scattering-angle dependency for transfer excitation of fast protons (300-1200 keV/u) colliding with helium ($p+He \rightarrow H + He^{+*}$). Our high-resolution fully differential data are accompanied by calculations, performed in the plane-wave first Born approximation and the eikonal wave Born approximation. Experimentally, we find a deep minimum in the differential cross section around 0.5 mrad. The comparison with our calculations shows that describing the scattering-angle dependence of transfer excitation in fast collisions requires us to go beyond the first Born approximation and in addition to use the initial state-wave function, which contains some degree of angular correlations.

*Electronic address: schoeffler@atom.uni-frankfurt.de

I. INTRODUCTION

From an experimental point of view, single-electron transfer has at least two interesting facets. First, it can be used as a tool for spectroscopy [1]. Energy gain spectroscopy and the related experiments in inverse kinematics exploit the recoil ion longitudinal momentum for Q -value determination (change in the electron binding energies). This allows us to investigate the energy levels of highly charged species and/or energy levels that do not decay radiatively or have long lifetimes. Second, the dynamics of the transfer process itself is of fundamental interest since it combines electron-electron dynamics, correlation, and questions of few-body momentum exchange.

While the ground-state charge transfer (CT), where no excitation is involved, hardly allows us to access these interesting questions, processes with two active electrons are much richer. Transfer ionization, where one electron is captured into a bound state of the projectile and a second one is released into the continuum, have been studied in great detail [2–14] and have led to a better understanding of initial and final state correlation [15–17]. Instead of being lifted to the continuum, the second target electron can also be promoted to a bound but excited state. This so-called transfer excitation (TE) has the experimental beauty that no electron needs to be detected, which can be extremely challenging especially at higher electron energies. An additional projectile-electron interaction or a shake-up lifts the electron into the excited state [18, 19].

In most of the theoretical and experimental studies the transfer into an excited state of the projectile or the transfer combined with an additional target excitation of a second electron was neglected. Especially at higher impact energies $E_p > 100$ keV/u, where the final electronic state determination in experiments is challenging or often impossible, the influence of excitation has not been investigated [20–23]. Projectile scattering angle distributions, which are final state selective, are rather rare [1, 24, 26–32]. All these measurements were only possible due to the development of a modern momentum imaging technique, cold target recoil ion momentum spectroscopy (COLTRIMS) combined with optimized three-dimensional focusing ion optics, which achieves longitudinal momentum resolution <0.04 a.u. (FWHM) [33]. This allows us to separate the final electronic states even for p-He collisions at energies as high as 1.2 MeV. In a previous publication we applied this high-resolution COLTRIMS and investigated the pure electron transfer, CT (i. e., without any excitation)

[33], while in the present paper we present scattering-angle-dependent cross sections for transfer excitation (i. e. the remaining target electron became excited).

The general theory of ion-atom collisions has been formulated for a long time by many authors, and one can find rather full reviews of the literature in [34–36]. We recall that the plane-wave first Born approximation (PWFBA) is valid only if the asymptotic wave functions in both the entrance and exit channels satisfy Dollard’s condition [37]. Fortunately, in the case of the particular reaction considered, $p + He \rightarrow H + He^{+*}$, these conditions are fulfilled. In the initial asymptotic state the charged proton does not interact with the neutral helium atom by long-range Coulomb force, and in the final asymptotic state the neutral hydrogen atom does not interact with the charged residual ion He^{+*} . In this case PWFBA \equiv CB1 (corrected first Born approximation) [35].

Recently, Madison and colleagues published a series of papers with calculations of the fully differential cross sections (FDSCS) for the transfer excitation reaction considered here at various energies [38]. A code for nine-dimensional (9D) numerical integration was used in this study. The results differed from the experiment by the factor v_p^4 . Some of the present authors showed in a comment [39] that this disagreement can be attributed to the quality of the numerical code [62]. We will add a more detailed discussion and new 9D results in Sec. III B below.

Here we consider the transfer excitation reaction $p + He \rightarrow H + He^{+*}$ at different high proton energies (300 - 1200 keV) and present both the experimental single differential cross sections for total excitation of the residual helium ion ($n \geq 2$) and the calculations within the PWFBA and the eikonal wave Born approximation (EWBA). Atomic units $\hbar = e = m_e = 1$ are used throughout unless otherwise specified.

II. EXPERIMENT

At the high impact velocities (3.5 - 7 a.u.) investigated here, the best energy loss and scattering-angle resolution is obtained by detecting the recoil-ion momentum instead of the momentum change of the projectile [24, 46]. This corresponds to a transformation from the projectile to the laboratory frame. In the present experiments we used the well-established COLTRIMS technique to measure both the neutral projectile H and the recoiling He^+ ion in coincidence [40–42]. The experiment has been performed at the 2.5 MV Van de

Graaff accelerator at the Institut für Kernphysik, Universität of Frankfurt. The proton beam was collimated with two sets of adjustable slits to a size of $0.5 \times 0.5 \text{ mm}^2$ at the interaction point. An electrostatic deflector placed upstreams of the target was used to remove beam impurities (H) by deflecting the primary beam slightly upwards. Behind the interaction region, right after leaving the spectrometer, another electrostatic deflector horizontally separated the primary beam of protons from the charge exchanged H. While the main proton beam ($\approx 1 \text{ nA}$) was dumped in a 0.5 m long Faraday cup, the neutral H projectiles were detected on a 40 mm position- and time-sensitive microchannel plate (MCP) detector with a delay line anode [43, 44] 5 m downstream of the target region. The target was provided by a two-stage supersonic gas jet of helium atoms. At the interaction point, the gas jet had a diameter of $\approx 1.5 \text{ mm}$ and an area density of $2 \times 10^{11} \text{ atoms/cm}^2$. The He^+ recoil ions produced in the overlap region of the gas jet and projectile beam were projected by a weak electrostatic field (9 V/cm) onto an 80-mm position- and time-sensitive MCP detector. To achieve the best possible momentum resolution, a three-dimensional time- and space focusing geometry was applied [19, 33, 45]. From the measured data, the time of flight (16 μs for He^+), and the position of impact, the initial three-dimensional momentum vector of the recoiling ion was derived. A momentum resolution $< 0.04 \text{ a.u.}$ in the longitudinal direction ($p_{||}$), in which the Q value of the reaction is encoded [see [24, 46]], was achieved (see Fig. 2(c) in [33]). The spectrometer geometry and electric fields yielded a 4π acceptance angle for all He^+ ions with momenta below 9 a.u.

In the plane perpendicular to the beam axis, we measured the scattering angle of the projectile and the transverse momentum of the recoiling ion. By momentum conservation they must add to zero, which was used for background suppression. The scattering angles presented below were deduced from the He^+ transverse momentum p_{\perp} , which has a far better momentum resolution ($< 0.1 \text{ a.u.}$) than the projectile. Gates on the different longitudinal momenta of the recoil ion ($p_{||}$) allow us to extract the scattering-angle distribution for a certain final electronic state [31]. The remaining tiny background of statistically false coincidences has been subtracted.

The data presented here (similar to [33]) show a significantly different scattering angle distribution than [22]. A notorious problem in most COLTRIMS measurements which might lead to differences in the results from different works is the calibration of the momentum. We therefore describe our calibration procedure in some detail to highlight its reliability on

a 1 % level. We choose our 1200 keV data set for this purpose. The position to momentum conversion along the beam direction (z) is based on the Q - $p_{||}$ relation ([24, 46]). As the Q value and the beam velocity are known on an absolute scale, the momentum can be calculated directly (see Fig. 2 in [33]). For the charge transfer reactions investigated here, the longitudinal momenta for the various final electronic states (no excitation or target or projectile or both being excited) differ in total by less than 0.5 a.u. Background events originate from a single ionization peak at $p_{||} = 0$ [25] and are therefore an excellent cross-check for our calibration on a larger scale. As can be seen from Fig. 1(a), the measured and calculated longitudinal momenta are in excellent agreement. A linear fit through these data points confirms the high quality of this calibration with a deviation of less than 1 %. This momentum is measured via the horizontal position of impact on the ion detector.

In the direction of the gas jet (y, vertical) the same position to momentum calibration factor was applied, utilizing the cylindrical symmetry of our spectrometer. The momentum in the time-of-flight (x) direction depends linearly on the electric field, which is known quite accurate and is additionally compared with SIMION simulations. Furthermore the physical symmetry around the beam axis was checked by comparing the momenta p_x (time-of-flight direction) and p_y (position direction). Figure 1(b) shows the transversal recoil ion momentum p_{\perp} vs. the corresponding azimuthal angle ϕ around the beam axis p_x/p_y . The physical symmetry is well reproduced, confirming the consistency of our momentum calibration in time-of-flight and position directions of our spectrometer.

III. THEORY

A. General formulas

Let us denote the projectile proton momentum by \vec{p}_p , the hydrogen momentum by \vec{p}_H , and the recoil-ion momentum by \vec{K} . We also define the transferred momentum as $\vec{q} = \vec{p}_H - \vec{p}_p$. The proton mass is $m_p = 1836.15$, the helium ion mass is $M \approx 4m_p$, and the ground-state energy $E_0^{He} = -2.903724377034$.

We choose very small scattering angles for the outgoing hydrogen ($0 \leq \theta_{p,lab} \lesssim 1.5$ mrad). It leads to a practically zero ion velocity K/M in the laboratory frame, and we can consider the ion as immovable during the reaction. The proton velocity $v_p = p_p/m_p$

and q vary about a few atomic units for a proton energy of several hundred keV. This fact allows us to neglect $K^2/2M$ and $q^2/2m_p$ everywhere they appear. Choosing the vector \vec{v}_p as the z axis, we obtain from the energy and momentum conservation for the longitudinal component $q_z = v_p/2 + Q_n/v_p$. The transverse component is $q_\perp = (\vec{p}_H)_\perp \approx m_p v_p \theta_{p,lab}$, and $Q_n = E_0^{He} - E_0^H - E_n^{ion}$.

The single differential cross section (SDCS) for TE processes takes the form

$$\frac{d\sigma_{ex}}{d\theta_{p,lab}} = 2 \frac{m_p^2 \theta_{p,lab}}{(2\pi)} \sum_{n=2}^{n-1} \sum_{l=0}^l \sum_{m=-l}^l |T_{nlm}|^2 \quad (1)$$

The factor 2 in (1) appears as a result of symmetrization of the final wave function.

The nonsymmetrized first Born approximation (FBA) matrix element in (1) is presented by the well-known 9D integral (see, for example, [48])

$$T_{nlm}^{FBA} \approx \int d^3 R e^{-i\vec{R}\vec{q}} \int d^3 \rho e^{i\vec{\rho}\vec{v}_p} \varphi_0(\rho) \int d^3 r_2 \phi_{nl}(r_2) Y_{lm}(\vec{r}_2) \left[-\frac{1}{\rho} - \frac{1}{|\vec{R} - \vec{r}_2|} + \frac{2}{R} \right] \Phi_0(\vec{R} - \vec{\rho}, \vec{r}_2). \quad (2)$$

The vector \vec{R} is the center of mass of the moving hydrogen subsystem at the end of reaction, $\vec{\rho}$ is the relative coordinate of electron 1 (transferred) in the hydrogen [described by the ground wave function $\varphi_0(\rho)$], and \vec{r}_2 is the relative coordinate of electron 2 in the He^+ subsystem (see details in [33, 47]). The hydrogen like excited (ground) wave function of the residual ion $\text{He}^+ \phi_{nl}(r) Y_{lm}(\vec{r})$ can be found in any text book.

Four different trial ground-state helium wave functions were used for the calculations. One is the loosely correlated $1s^2$ Roothaan-Hartree-Fock (RHF) wave function [49] (no angular correlation) with a rather poor ground-state energy of $E_{He}^{RHF} = -2.8617$ a.u. The second one [Silverman, Platas, and Matsen (SPM) [50]] includes angular correlations, but its ground energy $E_{He}^{SPM} = -2.8952$ is also far from the literature value. Two other trial functions are highly correlated. They are given in [51] with a ground-state energy of $E_{He}^{Ch} = -2.903721$ a.u. and [52], with a ground-state energy of $E_{He}^{Mitroy} = -2.9031$. Their energies are very close to the best-known ground-state energy. After the Fourier transformation of the wave functions in (2) we come to three-dimensional (ED) integrals for configuration interaction helium wave functions [49, 50, 52] and four-dimensional (4D) integrals for the function [51].

B. 9D integration

In the case of the SPM helium wave function we can also calculate EWBA matrix elements using the following code for 9D integration:

$$T_{nlm}^{EWBA} \approx \sqrt{2} \int d^3 R e^{-i\vec{R}\vec{q}} \int d^3 \rho e^{i\vec{\rho}\vec{v}_p} \varphi_0(\rho) \times \int d^3 r_2 \phi_{nl}(r_2) Y_{lm}(\vec{r}_2) e^{-(i/v_p) f(\vec{R}, \vec{\rho}, \vec{r}_2)} \left[-\frac{1}{\rho} - \frac{1}{|\vec{R} - \vec{r}_2|} + \frac{2}{R} \right] \Phi_0(\vec{R} - \vec{\rho}, \vec{r}_2), \quad (3)$$

with the eikonal phase factor

$$f(\vec{R}, \vec{\rho}, \vec{r}_2) = \ln \left[\frac{[v_p |\vec{R} - \vec{\rho}| + \vec{v}_p \cdot (\vec{R} - \vec{\rho})]^2 [v_p |\vec{R} - \vec{r}_2| + \vec{v}_p \cdot (\vec{R} - \vec{r}_2)]}{[v_p R + \vec{v}_p \cdot \vec{R}]^2 [v_p |\vec{R} - \vec{\rho} - \vec{r}_2| + \vec{v}_p \cdot (\vec{R} - \vec{\rho} - \vec{r}_2)]} \right]. \quad (4)$$

The way to get this phase factor can be found in [33].

Here we have to say a few words about 9D integration of oscillating functions. Chowdhury et al. recently presented a series of papers (see, for example, [53]) where they calculated 9D integrals the types in (2) and (3) for TE reactions. They obtained a discrepancy of a factor of 150 between theory and experiment at $E_p = 300$ keV. In [39, 54] some of the present authors have attributed this to a numerical problem of a non-optimal code of successive integration.

In our code we use the so-called adaptive subdivision method (ASM). Both the open Fortran codes [55, 56] and commercial ones [57] are available and written on the basis of the adaptive subdivision method. We modified these codes, and now they keep more data in the memory, can use the complex arithmetics, and are adapted for parallel calculations.

For the oscillating functions in (2) and (3) hyperspherical variables are used. In this case the integral by hyperradius is calculated analytically. The remaining 8D integral does not contain oscillations, and its domain of integration is restricted. For $E_p = 300$ keV the 8D integral is calculated with the relative accuracy $\epsilon = 0.1$. To approach this accuracy for $\theta_{p,lab} = 1$ mrad, it takes about 10^8 subregions of the ASM; 401 points of integration are taken in each subregion (so-called 7-point rule), i.e., about 21 points per variable.

C. Estimate of the residue in (1)

We note that the value Q_n satisfies an inequality $-2.403 < Q_n \leq -0.403$ for any $n \geq 1$. If we apply the closure approximation, i.e. replace $Q_n \rightarrow \bar{Q}$ in the sum by all bound states

with $-2.403 < \bar{Q} < -0.403$, we obtain, using the completeness condition of the Coulomb spectral functions,

$$\sum_{n=1}^{\infty} \sum_{l=0}^{n-1} \sum_{m=-l}^l |T_{nlm}|^2 = \int \frac{d^3k}{(2\pi)^3} |\langle \vec{k}|T \rangle|^2 - \int \frac{d^3k}{(2\pi)^3} |\langle \varphi^-(\vec{k})|T \rangle|^2. \quad (5)$$

The symbol $\langle \varphi^-(\vec{k})|T \rangle$ denotes the transfer ionization amplitude, where the emitted electron is described by a Coulomb wave [13, 14]; $\langle \vec{k}|T \rangle$ is the same, but the Coulomb wave is replaced by the plane wave. Here we have 6D and 7D integrals. We recall that in all integrals in (5) only \bar{Q} is used. Below we show that the presentation (5) allows us to estimate the residue of the sum in (1) beyond the exact calculations with a given n .

IV. RESULTS AND DISCUSSION

In Fig. 2 experimental and theoretical single-differential cross sections ($d\sigma/d\theta_{p,lab}$) for TE within the first Born approximation for various initial states are presented. Experimentally we can no distinguish between the different excited states; e.g., we sum over all $n \geq 2$. The integral of the electron transfer (with and without excitation) has been normalized to that in [58, 59]. TE contributes 4%-5% to the total electron transfer cross section, while the CT without any additional excitation amounts to 75%-80% [33]. The calculated and measured total cross sections (TCS) for TE, shown in Table I, are in good agreement only for the well correlated helium wave functions [51, 52]. The calculation based on a wave function without angular correlation completely fails. Obviously, TCS are defined mainly by the angle integration around the main peak in Fig. 2, where theory is close to the experiment for correlated helium wave functions. Comparing calculated and measured TCS has been the benchmark for testing theories. However, this is necessary but not sufficient.

The experimental distribution is overall similar to the one for CT without excitation [33] and exhibits two well-pronounced domains. Around 0.1 $mrad$ a sharp peak with a steep decrease is followed by a rather flat contribution for $\theta_{p,lab} > 0.5 mrad$. The peak at small angles originates from the momentum kick of the transferred electron [6, 60, 61]. If the captured electron is assumed to be at rest, the maximum possible proton scattering is 0.55 $mrad$; larger scattering angles require a momentum transfer between the nuclei. Especially, the minimum between these two contributions is more pronounced for TE than it is for CT. Also, the minimum is shifted slightly towards larger scattering angles ($\theta_{p,lab} = 0.45 mrad$

	Experiment (black dots)	Ref. [51] (black solid line)	RHF (red dashed line)	[52] (green dotted line)	Ref. SPM (blue dash-dotted line)
300 keV	1.093 a.u.	1.137 a.u.	0.8593 a.u.	1.150 a.u.	1.204 a.u.
630 keV	0.0404 a.u.	0.0581 a.u.	0.0204 a.u.	0.0581 a.u.	0.0616 a.u.
1000 keV	8.39×10^{-3} a.u.	7.08×10^{-3} a.u.	1.41×10^{-3} a.u.	7.16×10^{-3} a.u.	7.76×10^{-3} a.u.
1200 keV	2.79×10^{-3} a.u.	2.93×10^{-3} a.u.	4.79×10^{-4} a.u.	2.98×10^{-3} a.u.	3.29×10^{-3} a.u.

TABLE I: Total transfer excitation cross section for p+He collisions at 300-1200 keV impact energy. Experimental data have been normalized to published total electron transfer cross sections [58, 59]. Theoretical data are shown for various wave functions.

for CT, $\theta_{p,lab} = 0.5$ mrad for TE at 1.2 MeV). These findings contradict the measurements reported by Fischer et al. [22], who found the minimum at $\theta_{p,lab} = 0.35$ mrad for 1.3 MeV and have a narrower distribution in general. To exclude the most obvious possible source of error we have cross-checked that the calibration of our momenta is accurate within 1%, as described in Sec. II.

The minimum shows the boundary angle between the two main capture mechanisms. The shake-off amplitude (A_1+A_3); defined and explained in [13]) strongly depends on the electron-electron-correlations, defines the position and amplitude of the main peak, but goes down quickly. The sequential amplitude (A_2) is partially represented by the FBA but requires higher Born terms to be taken into account. The minimum defines some boundary between them. In the case of CT this minimum is sharp and equal zero for FBA. For TE it is not so sharp and is washed out by the excitation. But the minimum's origin remains the same. So we see that FBA (EWBA) can influence the amplitude and position of the main peak but not the position of the minimum. Calculations of higher Born terms are needed to account also for the sequential mechanism.

The experimental and the theoretical minima do not seem to be connected, especially as the experimental one shifts towards smaller angles with increasing projectile velocity. Therefore we speculate that the experimentally observed dip around 0.5 mrad can be explained in the following way. The broad contribution, peaking at larger scattering angles (1.5 mrad at 630 keV and 1.0 mrad at 1200 keV), may well be a result of the well-known Thomas-process (for details see Kim et al. [33] and references therein). This classical double-scattering

process ideally predicts a sharp peak at 0.47 mrad and was found to be around this value for very high energies [20–22]. At the rather low energies presented here, this peak might be shifted towards larger $\theta_{p,lab}$ due to an additional nucleus-nucleus scattering (N-N). From the strict geometrical conditions leading to Thomas-like electron capture, the momentum kick from the N-N scattering always points in the same direction as the initial kick with the electron. Hence the overall transverse momentum of the projectile $\theta_{p,lab}$ is the largest at small v_P , decreases for faster projectiles, and, finally, converges to the value of 0.47 mrad at an infinite projectile velocity.

We limit our calculations to $n \leq 3$ in the sum [Eq. (1)]. The shape of the SDCS is formed by three terms in Eq. (2), one of which (OBK) provides the direct $\text{He} \rightarrow e + \text{He}^+$ decay mechanism; the other two provide the double decay $\text{He} \rightarrow 2e + \text{He}^{2+}$ in the intermediate state. The shape in the case of helium wave functions with angular correlations (all except the red dashed line in Fig. 2) shows a the finite minimum very similar to the case $n = 1$ [33]. The wave function without angular correlations (red dashed line) fails completely. It is interesting to note that the SDCS calculated within the FBA for the CT practically does not depend on the trial helium wave function, and even the simplest $1s^2$ wave function describes the main peak [33] for the one-electron process quite well. The calculated total cross sections with angular correlated initial-state wave functions agree well with the experiment, as can be seen in Table I.

We also see that $E_p \sim 500$ keV is the lowest energy for which FBA still somehow describes the main peak at very small $\theta_{p,lab}$. For $E_p = 300$ keV the FBA fails completely. The FBA also fails to describe the position of the minimum and the behavior of the cross section beyond it. This is again in agreement with the conclusion drawn from CT (no excitation) in [33]. Calculations in the distorted-wave Born approximation or those performed in the second Born approximation are needed to describe the angular scattering in the regime where both the momentum transfer from the captured electron and the momentum exchange between the nuclei contribute.

We have tried to improve the description of the scattering by including an eikonal phase factor [Eq. (4)]. The results of this EWBA calculation for $E_p = 630, 1000$, and 1200 keV are presented in Figs. 3(a)-3(c). We use 9D integrals [Eq. (3)] with the SPM trial helium wave function and the eikonal phase factor (4). The positive (but very slow) progression of the main peak about 0.1 mrad towards the experiment is clearly visible. However, this EWBA

can not improve the situation at larger scattering angles; full second Born calculations are needed. We currently cannot perform these calculation for TE. For CT, however, second Born calculation are feasible. To illustrate the influence of the second Born approximation (SBA) on the angular scattering we present in Fig. 4 previously published [33] calculations in the first and second Born approximations together with EWBA calculations [Eq. (4)] for the CT reaction at 630 keV when the residual He^+ ion stays in its ground state ($n = 1$). While the EWBA considerably improves the agreement, the SBA calculations nearly perfectly describe the experimental data. Of course, the 9D numerical results fully coincide with 3D calculations of [Eq. (2)] and are close to the experiment, at least in its absolute scale.

In Fig. 5 the results of calculations with the approximation from [Eq. (10)] compared with exact calculations $n \leq 3$ are shown for two different wave functions [RHF in Figs. 5(a) and 5(c), and SPM in Figs. 5(b) and 5(d)]. In spite of rich behavior of the SDCS at very small scattering angles for different fitting parameters \bar{Q} , all curves merge into one bundle beyond some projectile-energy-dependent scattering angle. For $E_p = 1200$ keV it is about 0.6 *mrad*. That bundle has a different amplitude than the exact curve, but has a similar shape. This difference allows us to estimate a residue of the sum over excited states, for $n > 3$ to be about 10 % for the loosely correlated RHF wave function [Fig. 5(a) and (c)]. With the SPM wave function, which includes both radial and angular correrealation in figure 5 (b) and (d) we see practically no gap (about 1%-2%, and $n \leq 3$ calculations are enough to describe the angular spectrum).

In [19] the dynamical process that leads to a transfer excitation was investigated for collision energies 60-300 keV. The ratio of the transfer excitation and charge transfer ($R = TE/(TE+CT)$) of the single differential cross section $d\sigma/d\theta_{p,lab}$ was plotted. A peak around 0.4 *mrad* was found in collisions of p and He^{2+} colliding with helium. Similarly, in Fig. 6 the same ratio of transfer excitation and charge transfer for higher impact energies up to 1.2 MeV is plotted. Here a clear peak around 0.4 *mrad* can also be observed, which shifts towards smaller scattering angles with higher projectile energy. This peak arises because the energy transfer necessary for the excitation goes along with a momentum transfer from the projectile to the electron to be excited, which is also in the transverse direction [2]. This shifts the scattering angle to larger values, approaching 0.55 *mrad*, the maximum scattering angle of a proton at an electron. For large scattering angles the scattering is caused by the momentum transfer between the nuclei, and hence CT and TE show a similar fall off.

In Fig. 6(e) we present the ratio R for EWBA and PWFBA calculations when the helium function is highly correlated. The angle domain $0 < \theta_{p,lab} < 0.4 \text{ mrad}$ is the most interesting for a comparison of theory and experiment in the case of our simple approximations. Here we are still near the main peak for both TE and CT reactions. We see that the agreement with the experiment is rather poor if PWFBA is used. However, EWBA describes the domain of interest much better. It is a good sign that this approximation improves the description of the SDCS in the vicinity of main peaks at high impact energies.

V. CONCLUSIONS

In conclusion, we present experimental data of the cross-section differential in the scattering angle and the corresponding FBA theory for transfer excitation in proton-helium collision at 300, 630, 1000, and 1200 keV. Our calculations have been carried out using the plane-wave first Born approximation with $1s^2$ and highly correlated trial helium wave functions. We find that this two-electron process cannot be described using a $1s^2$ wave function. All wave functions including angular correlations give rather similar scattering-angle distributions. All fail to describe the experiment for most scattering angles. Including an eikonal factor does not solve this problem. Calculations for capture without excitation show that a second Born theory describes the scattering correctly, at least for this channel. The projectile scattering is determined by an interplay of the momentum exchange of the projectile with the target nucleus, the electron which is captured, and the electron which is excited. Thus a theory capable of describing this process must include an angularly correlated initial-state wave function as well as second- or higher-order Born terms.

VI. ACKNOWLEDGMENTS

We acknowledge financial support from the Deutsche Forschungsgemeinschaft (DFG), Grant No. SCHO 1210/2-1. A.G.G. is grateful to the Dynasty Foundation for the partial financial support. This work was also partially supported by the Russian Foundation of Basic Research (RFBR), Grant No. 11-01-00523-a. All calculations were performed at the Moscow State University Research Computing Centre (supercomputers Lomonosov and Chebyshev) and the Joint Institute for Nuclear Research Central Information and Computer

Complex. The authors are grateful to Dž. Belkić for inspiring discussions and help.

- [1] D. Fischer, B. Feuerstein, R. D. DuBois, R. Moshammer, J. R. Crespo Lopez-Urrutia, I. Draganic, H. Lörch, A. N. Perumal and J. Ullrich, *J. Phys. B*, **35**, 1369-1377, (2002)
- [2] E. Horsdal, B. Jensen, and K.O. Nielsen, *Phys. Rev. Lett.*, **57**, 1414, (1986)
- [3] J. Palinkas, R. Schuch, H. Cederquist, and O. Gustafsson, *Phys. Rev. Lett.*, **63**, 2464, (1989)
- [4] R. Hippler, G. Schiawietz, J. Bossler, *Phys. Rev. A*, **35**, 485, (1987)
- [5] R. Shingal and C. D. Lin, *J. Phys. B*, **24**, 251, (1991)
- [6] V. Mergel, R. Dörner, M. Achler, K. Khayyat, S. Lencinas, J. Euler, O. Jagutzki, S. Nüttgens, M. Unverzagt, L. Spielberger, W. Wu, R. Ali, J. Ullrich, H. Cederquist, A. Salin, C. J. Wood, R. E. Olson, Dž. Belkić, C. L. Cocke and H. Schmidt-Böcking, *Phys. Rev. Lett.*, **79**, 387, (1997)
- [7] O. Woitke, P. A. Zavodszky, S. M. Ferguson, J. H. Houck and J. A. Tanis, *Phys. Rev. A*, **57**, 2692, (1998)
- [8] V. Mergel, R. Dörner, K. Khayyat, M. Achler, T. Weber, O. Jagutzki, H. J. Lüdde, C. L. Cocke and H. Schmidt-Böcking, *Phys. Rev. Lett.*, **86**, 2257, (2001)
- [9] H.T. Schmidt, A. Fardi, R. Schuch, S.H. Schwartz, H. Zettergren, H. Cederquist, L. Bagge, H. Danared, A. Källberg, J. Jensen, K.-G. Rensfelt, V. Mergel, L. Schmidt, H. Schmidt-Böcking, and C.L. Cocke, *Phys. Rev. Lett.*, **89**, 163201, (2002)
- [10] M. Schöffler, A. L. Godunov, C. T. Whelan, H. R. J. Walters, V. S. Schipakov, V. Mergel, R. Dörner, O. Jagutzki, L. Ph. H. Schmidt, J. Titze, E. Weigold and H. Schmidt-Böcking, *J. Phys. B*, **38**, L123, (2005)
- [11] A. L. Godunov, C. T. Whelan, H. R. J. Walters, V. S. Schipakov, M. Schöffler, V. Mergel, R. Dörner, O. Jagutzki, L. Ph. H. Schmidt, J. Titze, and H. Schmidt-Böcking, *Phys. Rev. A*, **71**, 052712, (2005)
- [12] M. Schulz, X. Wang, M. Gundmundsson, K. Schneider, A. Kelkar, A. B. Voitkiv, B. Najjari, M. Schöffler, L. Ph. H. Schmidt, R. Dörner, J. Ullrich, R. Moshammer and D. Fischer, *Phys. Rev. Lett.*, **108**, 043202, (2012)
- [13] M. S. Schöffler, O. Chuluunbaatar, Yu. V. Popov, S. Houamer, J. Titze, T. Jahnke, L. Ph. H. Schmidt, O. Jagutzki, A. G. Galstyan, and A. A. Gusev, *Phys. Rev. A*, **87**, 032715, (2013)

[14] M. S. Schöffler, O. Chuluunbaatar, S. Houamer, A. Galstyan, J. N. Titze, L. Ph. H. Schmidt, T. Jahnke, H. Schmidt-Böcking, R. Dörner, Yu. V. Popov, A.A. Gusev, and C. Dal Cappello, Phys. Rev. A **88**, 042710, (2013).

[15] T. Y. Shi and C. D. Lin, Phys. Rev. Lett, **89**, 163202, (2002)

[16] H. Schmidt-Böcking, V. Mergel, R. Dörner, C. L. Cocke, O. Jagutzki, L. Schmidt, Th. Weber, H.J. Lüdde, E. Weigold, J. Berakdar, H. Cederquist, H.T. Schmidt, R. Schuch, and A. S. Kheifets, Europhys. Lett., **62**, 477, (2003)

[17] A. Godunov, C. T. Whelan, and H. R. J. Walters, J. Phys. B, **37**, L201, (2004)

[18] K. M. Dunseath and D. S. F. Crothers, J. Phys. B, **24**, 5003, (1991)

[19] M. S. Schöffler, J. N. Titze, L. Ph. H. Schmidt, T. Jahnke, O. Jagutzki, H. Schmidt-Böcking and R. Dörner, Phys. Rev. A., **80**, 042702, (2009)

[20] E. Horsdal-Pedersen, C. L. Cocke and M. Stöckli, Phys. Rev. Lett., **50**, 1910, (1983)

[21] D. Fischer, K. Stochkel, H. Cederquist, H. Zettergren, P. Reinhed, R. Schuch, A. Kallberg, A. Simonsson and H. T. Schmidt, Phys. Rev. A, **73**, 052713, (2006)

[22] D. Fischer, M. Gudmundsson, Z. Berenyi, N. Haag, H. A. B. Johansson, D. Misra, P. Reinhed, A. Källberg, A. Simonsson, K. Stochkel, H. Cederquist and H. T. Schmidt, Phys. Rev. A, **81**, 012714, (2010)

[23] M. Gudmundsson, D. Fischer, N. Haag, H. A. B. Johansson, D. Misra, P. Reinhed, H. Schmidt-Böcking, R. Schuch, M. Schöffler, K. Stochkel, H. T. Schmidt and H. Cederquist, J. Phys. B, **43**, 185209, (2010)

[24] V. Mergel, R. Dörner, J. Ullrich, O. Jagutzki, S. Lencinas, S. Nüttgens, L. Spielberger, M. Unverzagt, C. L. Cocke, R. E. Olson, M. Schulz, U. Buck, E. Zanger, W. Theisinger, M. Isser, S. Geis, and H. Schmidt-Böcking, Phys. Rev. Lett., **74**, 2200, (1995)

[25] R. Dörner, V. Mergel, L. Zaoyuan, J. Ullrich, L. Spielberger, R.E. Olson, H. Schmidt-Böcking, J. Phys. B **28**, 435, (1995)

[26] R. Dörner, V. Mergel, L. Spielberger, O. Jagutzki, J. Ullrich and H. Schmidt-Böcking, Phys. Rev. A, **57**, 312, (1998)

[27] M. A. Abdallah, W. Wolff, H. E. Wolf, E. Sidky, E. Y. Kamber, M. Stöckli, C. D. Lin and C. L. Cocke, Phys. Rev. A, **57**, 4373, (1998)

[28] M. A. Abdallah, W. Wolff, H. E. Wolf, E. Y. Kamber, M. Stöckli and C. L. Cocke, Phys. Rev. A, **58**, 2911 (1998)

- [29] E. Y. Kamber, M. A. Abdallah, C. L. Cocke and M. Stöckli, Phys. Rev. A, **60**, 2907, (1999)
- [30] H. Zhang, X. Flechard, A. Cassimi, L. Adoui, G. Cremer, F. Fremont and D. Hennecart, Phys. Rev. A, **64**, 012715, (2001)
- [31] M. S. Schöffler, J. Titze, L. Ph. H. Schmidt, T. Jahnke, N. Neumann, O. Jagutzki, H. Schmidt-Böcking, R. Dörner and I. Mancev, Phys. Rev. A, **79**, 064701, (2009)
- [32] S. Knoop, D. Fischer, Y. Xue, M. Zapukhlyak, C. J. Osborne, Th. Ergler, T. Ferger, J. Braun, G. Brenner, H. Bruhns, C. Dimopoulou, S. W. Epp, A. J. Gonzalez Martinez, G. Sikler, R. Soria Orts, H. Tawara, T. Kirchner, J. R. Crespo Lopez-Urrutia, R. Moshammer, J. Ullrich and R. Hoekstra, J. Phys. B, **41**, 195203, (2008)
- [33] Hong-Keun Kim, M. S. Schöffler, S. Houamer, O. Chuluunbaatar, J. N. Titze, L. Ph. H. Schmidt, T. Jahnke, H. Schmidt-Böcking, A. Galstyan, Yu. V. Popov and R. Dörner, Phys. Rev. A, **85**, 022707, (2012)
- [34] Dž. Belkić, I. Mančev, and J. Hanssen, Rev. Mod. Phys., **80**, 249, (2008)
- [35] Dž. Belkić, R. Gayet, and A. Salin, Phys. Rep., **56**, 281, (1979).
- [36] Dž. Belkić, *Quantum Theory of High-Energy IonAtom Collisions* (Taylor and Francis, London, 2008)
- [37] J. Dollard, J. Math. Phys. **5**, 729 (1964).
- [38] A.L. Harris, J.L. Peacher, and D.H. Madison and J. Colgan, Phys. Rev. A, **80**, 062707 (2009); U. Chowdhury, A.L. Harris, J.L. Peacher, and D.H. Madison, J. Phys. B, **45**, 035203, 175204 (2012).
- [39] S. Houamer and Yu. V. Popov, J. Phys. B, **46**, 028001 (2013)
- [40] J. Ullrich, R. Moshammer, R. Dörner, O. Jagutzki, V. Mergel, H. Schmidt-Böcking and L. Spielberger, J. Phys. B, **30**, 2917, (1997)
- [41] R. Dörner, V. Mergel, O. Jagutzki, L. Spielberger, J. Ullrich, R. Moshammer and H. Schmidt-Böcking, Physics Reports, **330**, 95, (2000)
- [42] J. Ullrich, R. Moshammer, A. Dorn, R. Dörner, L. Ph. H. Schmidt and H. Schmidt-Böcking, Rep. Prog. Phys., **66**, 1463, (2003)
- [43] O. Jagutzki, J. S. Lapington, L. B. C. Worth, U. Spillman, V. Mergel and H. Schmidt-Böcking, Nucl. Instr. and Meth. in Phys. Res. A, **477**, 256, (2002)
- [44] O. Jagutzki, V. Mergel, K. Ullmann-Pfleger, L. Spielberger, U. Spillmann, R. Dörner and H. Schmidt-Böcking, Nucl. Instr. and Meth. in Phys. Res. A, **477**, 244, (2002)

[45] R. Dörner, V. Mergel, L. Spielberger, M. Achler, Kh. Khayyat, T. Vogt, H. Bräuning, O. Jagutzki, T. Weber, J. Ullrich, R. Moshammer, M. Unverzagt, W. Schmitt, H. Khemliche, M. H. Prior, C. L. Cocke, J. Feagin, R. E. Olson, and H. Schmidt-Böcking, Nucl. Instrum. and Methods in Phys. Res. B, **124**, 225, (1997)

[46] R. Ali, V. Frohne, C. L. Cocke, M. Stockli, S. Cheng, and M. L. A. Raphaelian, Phys. Rev. Lett., **69**, 2491, (1992)

[47] S. Houamer, Yu. V. Popov, and C. Dal Cappello, Phys. Rev. A **81**, 032703, (2010)

[48] J. D. Jackson and H. Schiff, Phys. Rev., **89**, 359, (1953)

[49] E. Clementi and C. Roetti. Atomic Data and Nuclear Data Tables **14**, 177, (1974)

[50] J.N. Silverman *et al.* J. Chem. Phys. **32**, 1402, (1960)

[51] O. Chuluunbaatar *et al.*, Phys. Rev. A **74**, 014703, (2006)

[52] J. Mitroy, I. E. McCarthy, and E. Weigold, J. Phys. B **18**, 4149, (1985)

[53] U. Chowdhury *et al.*, J. Phys. B **45**, 035203 (2012)

[54] U. Chowdhury *et al.*, J. Phys. B **46**, 028002 (2013)

[55] <http://crantastic.org/packages/adapt>

[56] <http://www.stat.duke.edu/courses/Spring02/sta376/eg/lc/dcuhre.f>

[57] <http://www.nag.com/>

[58] J. F. Williams, Phys. Rev., **157**, 97, (1967)

[59] M. B. Shah, P. McCallion and H. B. Gilbody, J. Phys. B, **22**, 3037 (1989)

[60] E. Y. Kamber, C. L. Cocke, S. Cheng and S. L. Varghese, Phys. Rev. Lett., **60**, 2026, (1988)

[61] R. Dörner, J. Ullrich, H. Schmidt-Böcking and R. E. Olson, Phys. Rev. Lett., **63**, 147, (1989)

[62] Recently D. Madison communicated that they found another reason for such a disagreement.

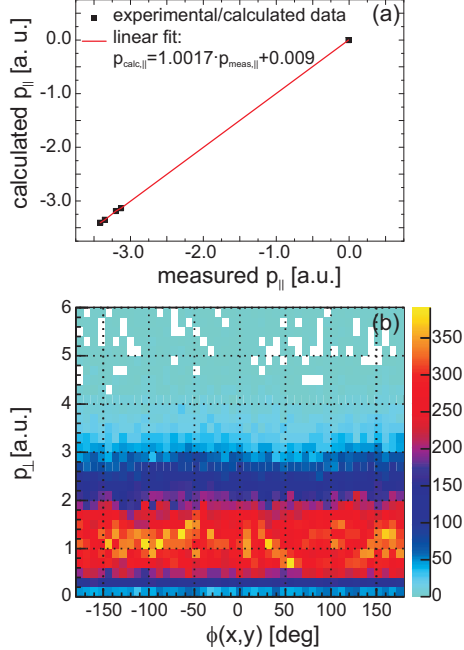


FIG. 1: (Color online) Check of the experimental calibration for electron transfer in p+He collisions at 1200 keV. (a) Measured longitudinal ($p_{||}$) momentum of the distinguishable four final states for electron transfer and single ionization (peaking at zero). An additional linear fit through the data points shows the accuracy of the $p_{||}$ calibration. (b) ϕ angle around the beam axis vs. transversal momentum p_{\perp} , showing the proper calibration of the time-of-flight and position direction for electron transfer.

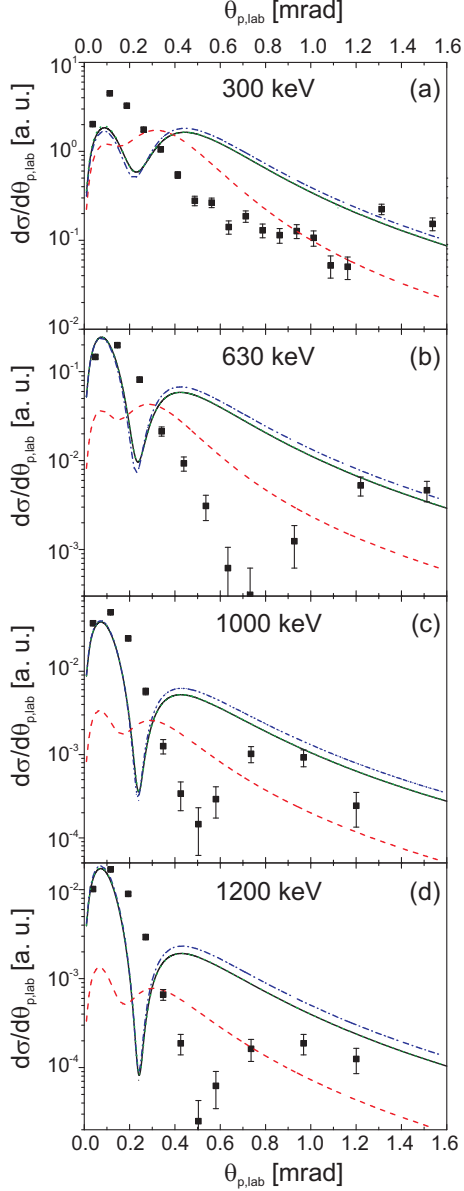


FIG. 2: (Color online) Experimental and theoretical data for the scattering-angle-dependent transfer excitation in $p+He$ collisions. Squares are the experimental points with statistical error bars, the dashed red line is the RHF [49] trial helium wave function, the dash-dotted blue line is the SPM [50] wave function, the solid black line [51] and the dotted green line [52] practically coincide. Experimental data have been normalized to published total electron transfer cross sections [58, 59]. (a) 300 keV, (b) 630 keV, (c) 1000 keV and (d) 1200 keV incident proton energy. Experimental error bars show the statistical standard deviation.

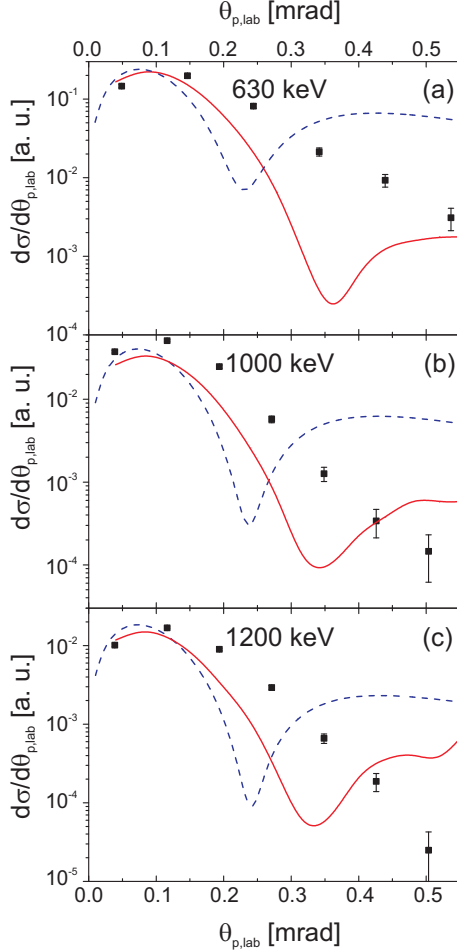


FIG. 3: (Color online) Experimental and theoretical data for the scattering-angle-dependent transfer excitation in p+He collisions for (a) 630 keV, (b) 1000 keV, and (c) 1200 keV impact energy. SPM FBA calculations are supplemented by the eikonal phase factor. Dashed blue line: SPM; solid red line: SPM with the 4C phase factor; full squares: experimental data (same as in Fig. 2).

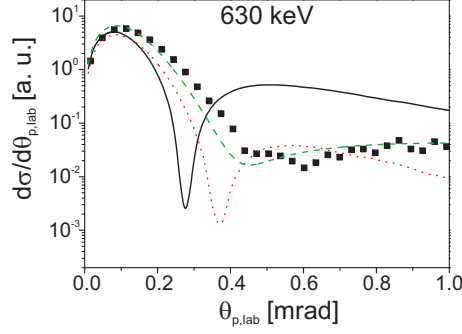


FIG. 4: (Color online) SDCS vs. the scattering angle $\theta_{p,lab}$ for the CT process leaving the helium ion in its ground state $n = 1$. The RHF helium wave function is used. Solid black line: FBA; dashed green line: SBA (taken from [33], Fig. 3, $\bar{E} = 0.1$); dotted red line: EWBA; squares: experiment [33]. $E_p = 630$ keV.

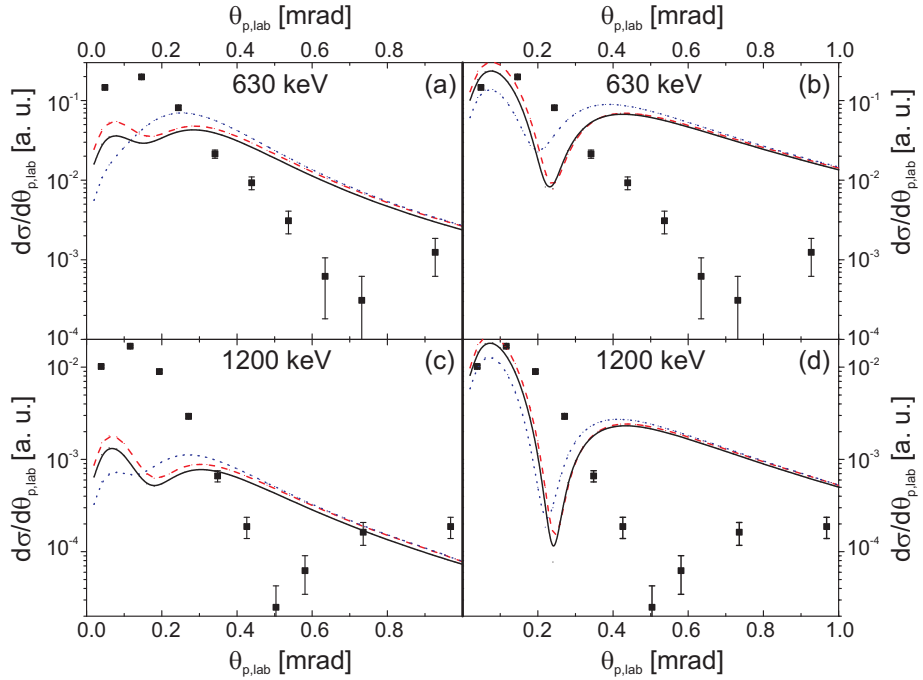


FIG. 5: (Color online) SDCS vs. the scattering angle $\theta_{p,lab}$ for the TE process for (a) and (b) 630 keV and (c) and (d) 1200 keV. The RHF wave function is used for the calculations in (a) and (c), while the SPM wave function is used in (b) and (d). Solid black line: Eq. (5) with $n=2+3$; dotted blue line: Eq. (10) with $\bar{Q}=-0.403$ a.u.; dashed red line: Eq. (10) with $\bar{Q}=-2.403$ a.u.; squares: experimental data.

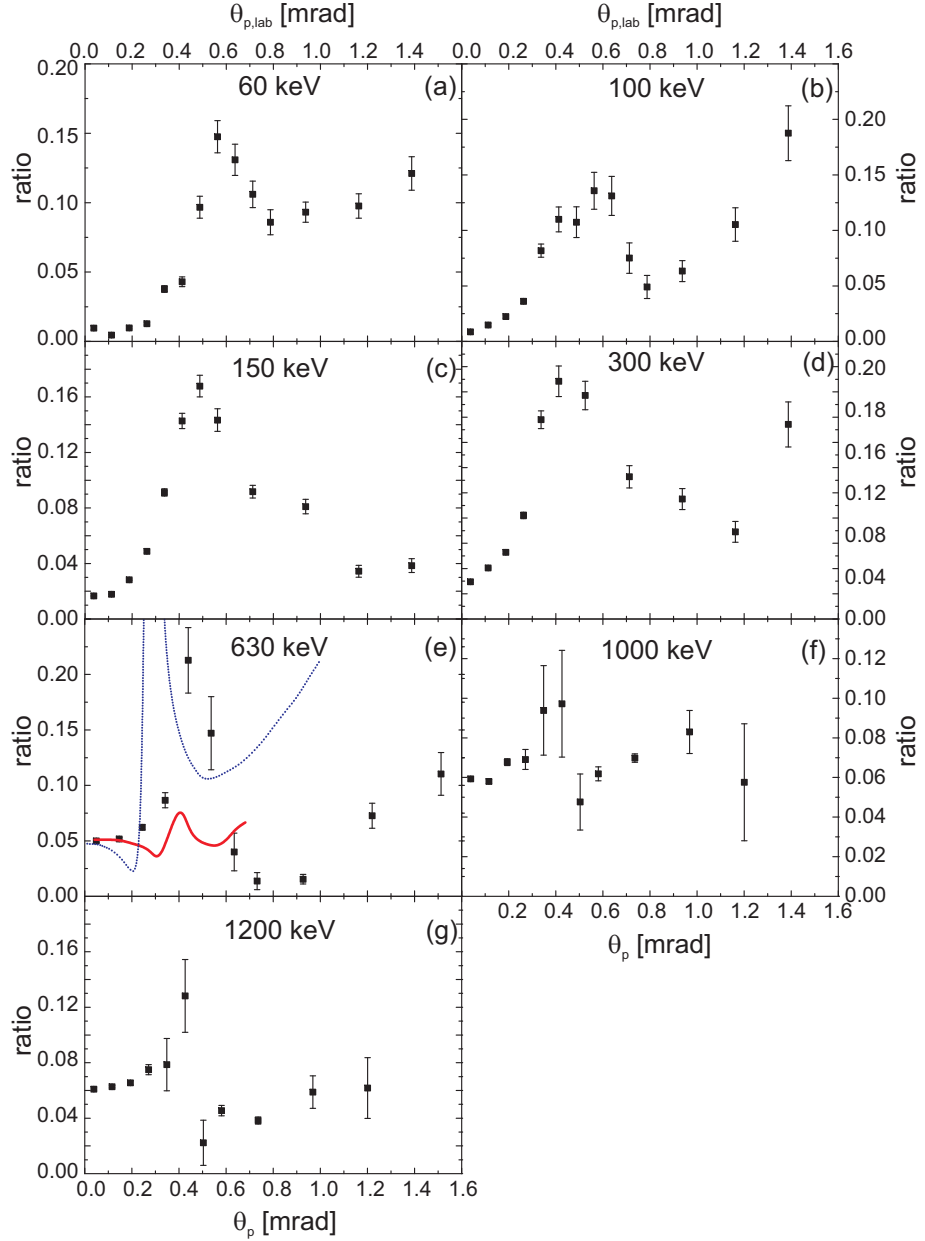


FIG. 6: (Color online) Ratio of transfer excitation and charge transfer of the differential cross section $d\sigma/d\theta_{p,lab}$ in $p+He$ collisions at projectile energies of 60-1200 keV. Datapoints for (a)-(d) were taken from [19]. Black squares are the experimental points. The solid red line in (e) represents an EWBA and the dotted blue line represents a PWFB calculation.